

# We are IntechOpen, the world's leading publisher of Open Access books Built by scientists, for scientists

6,900

Open access books available

186,000

International authors and editors

200M

Downloads

Our authors are among the

154

Countries delivered to

TOP 1%

most cited scientists

12.2%

Contributors from top 500 universities



WEB OF SCIENCE™

Selection of our books indexed in the Book Citation Index  
in Web of Science™ Core Collection (BKCI)

Interested in publishing with us?  
Contact [book.department@intechopen.com](mailto:book.department@intechopen.com)

Numbers displayed above are based on latest data collected.  
For more information visit [www.intechopen.com](http://www.intechopen.com)



# Wireless Optical Nanolinks with Yagi-Uda and Dipoles Plasmonic Nanoantennas

*Karlo Queiroz da Costa, Gleida Tayanna Conde de Sousa,  
Paulo Rodrigues Amaral, Janilson Leão Souza,  
Tiago Dos Santos Garcia and Pitther Negrão dos Santos*

## Abstract

In this work, we present a theoretical analysis of wireless optical nanolinks formed by plasmonic nanoantennas, where the antennas considered are Yagi-Uda and cylindrical nanodipoles made of Au. The numerical analysis is performed by the finite element method and linear method of moments, where the transmission power and the near electric field are investigated and optimized for three nanolinks: Yagi-Uda/Yagi-Uda, Yagi-Uda/dipole and dipole/dipole. The results show that all these cases can operate with good transmission power at different frequencies by adjusting the impedance matching in the transmitting antennas and the load impedance of the receiving antennas.

**Keywords:** nanoplasmonic, nanoantennas, wireless optical nanolink, power transmission

## 1. Introduction

The electromagnetic scattering of metals in optical frequency region possesses special characteristics. At these frequencies, there are electron oscillations in the metal called plasmons with distinct resonant frequencies, which produce strongly enhanced near fields at the metal surface. This effect can be analyzed using Lorentz-Drude model of the complex dielectric constant. The science of the electromagnetic optical response of metal nanostructures is known as plasmonics or nanoplasmonics [1, 2].

One subarea of nanoplasmonics is the field of optical nanoantennas, which are metal nanostructures used to transmit or receive optical fields [3–5]. This definition is similar to that of conventional radio frequency (RF) and microwave antennas. The main difference between these two regimes (RF-microwave and optical) is due to physical properties of the metals at optical frequencies where they cannot be considered as perfect conductors because of the plasmonic effects [2]. Comprehensive reviews on optical antennas have been presented in [6–11]. In these works, the authors described recent developments in calculation of such antennas, their applications and challenges in their design. In **Figure 1**, we present some examples of fabricated nanoantennas.

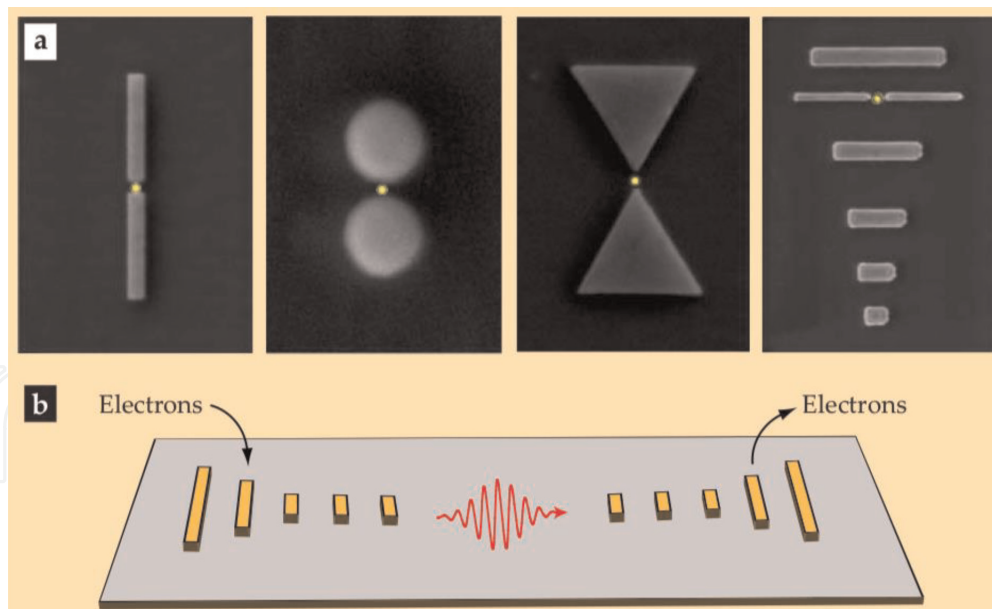


**Figure 1.**

(a) Scanning electron micrographs of various optical nanoantennas. (b) Application example of Yagi-Uda nanoantennas in wireless optical nanolink, where the nanoantennas perform transduction between electrical current and optical radiation [5].

Optical nanoantennas have received great interest in recent years in the scientific community due to their ability to amplify and confine optical fields beyond the light diffraction limit [6]. With this characteristic, it is possible to apply in several areas, such as nanophotonics, biology, chemistry, computer science, optics and engineering, among others [6, 7, 12]. In addition, these studies were expanded due to the development of computational numerical methods and innovations in nanofabrication techniques, such as electron beam lithography, colloidal lithography and ion beam lithography [9].

Optical wireless nanolinks with nanoantennas can be used to efficiently communicate between devices, significantly reducing the losses that occur in wired communication. Nanolinks with different geometries of nanoantennas were investigated in the literature [13–17]. In [13] the authors propose a broadband nanolink formed by dipole-loop antennas. The results showed that using this nanolink with dipole-loop antennas instead of conventional dipoles, it is possible to increase the operating bandwidth of the system to the range of 179.1–202.5 THz, which is within the optical range of telecommunications. In [14], a wireless nanolink formed by dipole antennas is compared to a wired nanolink formed by a waveguide, the study showed that the wireless link may work better than a plasmon waveguide in sending optical signal in nanoscale from one point to another, from a certain distance. In [15], a nanolink Yagi-Uda chip directives are proposed, the results show that the use of directional antennas increases the energy transfer (power ratio) and link efficiency, minimizing interference with other parts of the circuit. In [16], it is presented another wireless nanolink application formed by a transmitting nanoantenna Vivaldi and another receiver, to be used in chip, with that nanolink a high gain and bandwidth covering the entire spectrum of the C band of telecommunications. In [17], broadband nanolinks were analyzed using horn and dipole type optical nanoantennas, where the horn antenna had better performance, because better energy transfer at the nanolink and greater bandwidth were obtained in relation to the dipole link. These studies used identical transmitting and receiving antennas, and showed the feasibility of using wireless communication in the nanophotonics.

In this work, we present a comparative analysis of nanolinks formed by equal and different transmitting and receiving nanoantennas. The antennas used are

Yagi-Uda and dipole. The numerical analysis is performed by the method of moments (MoM) [18] and the finite element method (FEM) through the software COMSOL Multiphysics [19]. In this analysis, the transmission power and the near electric field are investigated for three nanolinks: Yagi-Uda/dipole, Yagi-Uda/Yagi-Uda and dipole/dipole. This work is organized as follow: Section 1 is the introduction, Section 2 presents the description of nanolinks, Section 3 presents the numerical model used in the analysis, Section 4 contain the numerical results, and Section 5 are the conclusions.

## 2. Description of nanolinks

In this work, three models of nanolinks are proposed and analyzed. The first is a nanolink formed by dipole/dipole antennas (**Figure 2**, without reflector and directors), the second by Yagi-Uda/dipole antennas (**Figure 2**) and the third by Yagi-Uda/Yagi-Uda antennas (**Figure 2**, with the receiving antenna equal to the transmitting antenna).

The geometry of the Yagi-Uda/dipole nanolink is presented in **Figure 2**, where a voltage source  $V_S$  excites the left nanoantenna, which functions as a transmitter (Yagi-Uda) and the right nanoantenna that acts as a receptor (dipole), connected to load impedance  $Z_C$ . The nanolink is located in the free space and is formed by cylindrical conductors of gold. The complex permittivity of this material is represented by the Lorentz-Drude model of Au [11]. The Yagi-Uda transmitting nanoantenna is composed of a dipole, a reflector and three directors (**Figure 1** left). The dipole of the transmitter, located in the  $z = 0$  plane along the  $x$ -axis and centered at the origin, has total length  $2h_{dT} + d_{dT}$ , radius  $a_{dT}$  and voltage gap  $d_{dT}$ . The reflector has  $h_r$  length and  $a_r$  radius. The directors have the same length  $h_d$  and radius  $a_d$ . The parameters  $d_{hr}$  and  $d_{hd}$  are the distances between reflector and directors element to Yagi-Uda antenna, respectively (**Figure 1** left). The receiver antenna is a dipole (**Figure 1** right), located in the  $z = 0$  plane and displaced at a  $d_{TR}$  relative to the dipole axis of the transmitting antenna, with total length  $2h_{dR} + d_{dR}$ , radius  $a_{dR}$ , gap length  $d_{dR}$  and load  $Z_C$  connected to its gap.

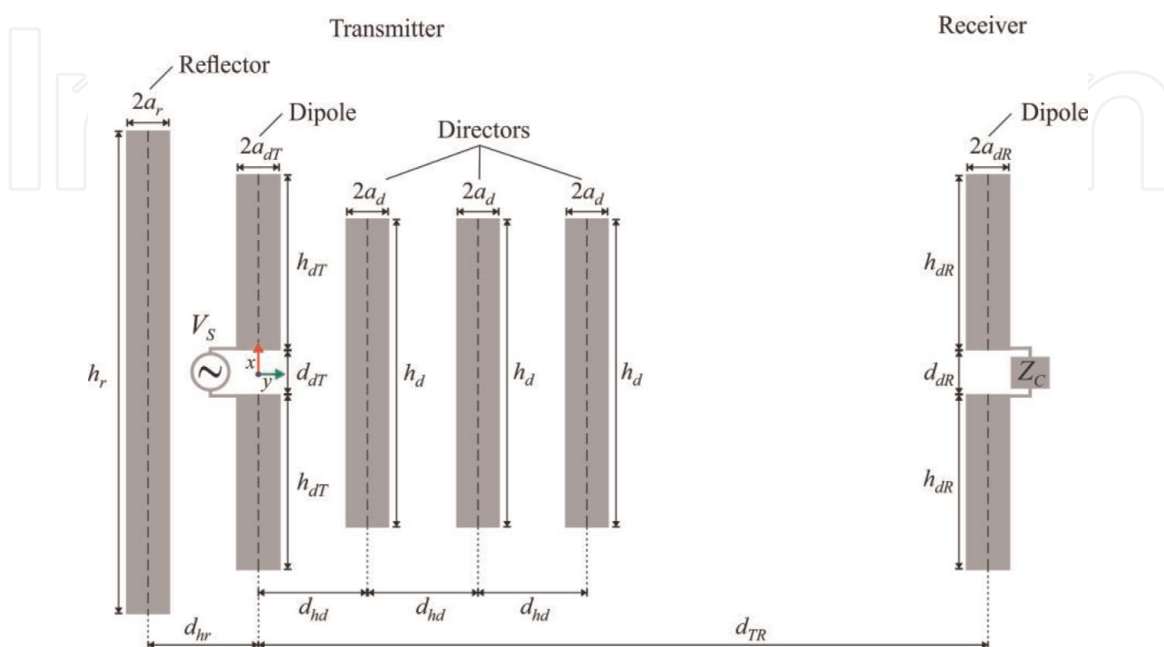


**Figure 2.** Geometry of the nanolink composed by a Yagi-Uda antenna (transmitter) and a nanodipole (receiver).

### 3. Numerical model

In this section, we present the numerical methods used in the analysis of the wireless optical nanolinks described in the last section. The methods used here are MoM [18] and FEM [19].

#### 3.1 Method of moments

The linear MoM presented here is based in the linear current approximation with an equivalent surface impedance model of the cylindrical conductors, with sinusoidal test and base functions [18]. The method will be explained for the particular example of a single dipole radiating in a free space, composed by plasmonic cylindrical elements made of gold.

**Figure 3** shows the geometry of the original problem, the equivalent MoM and circuit models of the nanodipole. In this figure,  $L$  is the length of the arms,  $d$  is the nanodipole gap and  $a$  is the dipole radius. The total length of this antenna is  $L_t = 2L + d$ . In present analysis, we do not take into account the capacitance generated by the air gap ( $C_{gap}$ ) of the nanodipole. In this case, our input impedance is equivalent to that  $Z_a$  presented in [20] without  $C_{gap}$ .

In the radiation problem of **Figure 3**, the gold material of the antenna is represented by the Lorentz-Drude model for complex permittivity  $\epsilon_{Au} = \epsilon_0 \epsilon_{rAu}$ :

$$\epsilon_{rAu} = \epsilon_\infty - \frac{\omega_{p1}^2}{\omega^2 - j\Gamma\omega} + \frac{\omega_{p2}^2}{\omega_0^2 - \omega^2 + j\gamma\omega}, \quad (1)$$

where the parameters in this equation are as follows [1]:  $\epsilon_\infty = 8$ ,  $\omega_{p1} = 13.8 \times 10^{15} \text{s}^{-1}$ ,  $\Gamma = 1.075 \times 10^{14} \text{s}^{-1}$ ,  $\omega_0 = 2\pi c/\lambda_0$ ,  $c = 3 \times 10^8 \text{ m/s}$ ,  $\lambda_0 = 450 \text{ nm}$ ,  $\omega_{p2} = 45 \times 10^{14} \text{s}^{-1}$ ,  $\gamma = 9 \times 10^{14} \text{s}^{-1}$ , and  $\omega$  is the angular frequency in rad/s. **Figure 4** presents the real and imaginary part of (1) versus wavelength ( $\lambda$ ). This figure also shows the experimental data of [21]. We observe a good agreement between the results of the Lorentz-Drude model of (1) and the experimental data for  $\lambda > 500 \text{ nm}$ .

The losses in metal are described by the surface impedance  $Z_s$ . This impedance can be obtained approximately by considering cylindrical waveguide with the mode  $\text{TM}_{01}$ . In this case, the surface impedance is given by [22].

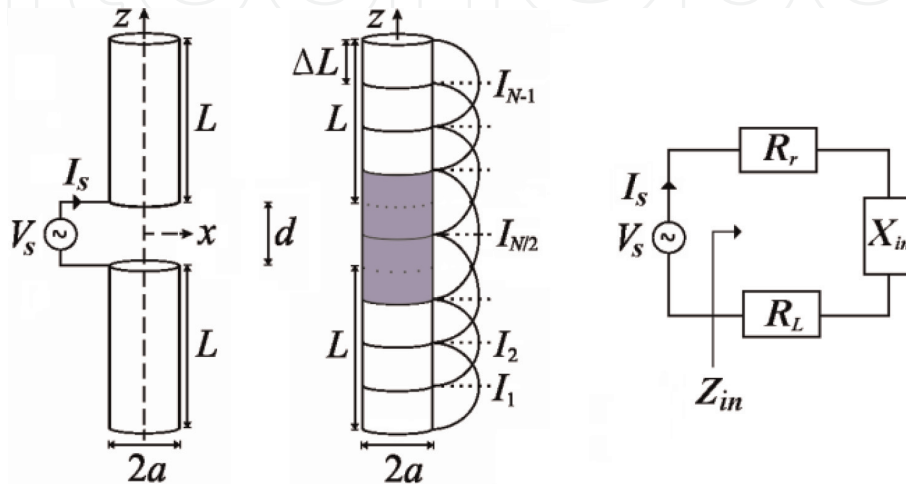


**Figure 3.** Geometry of nanodipole: original problem (left), MoM model (middle), and equivalent circuit model (right).

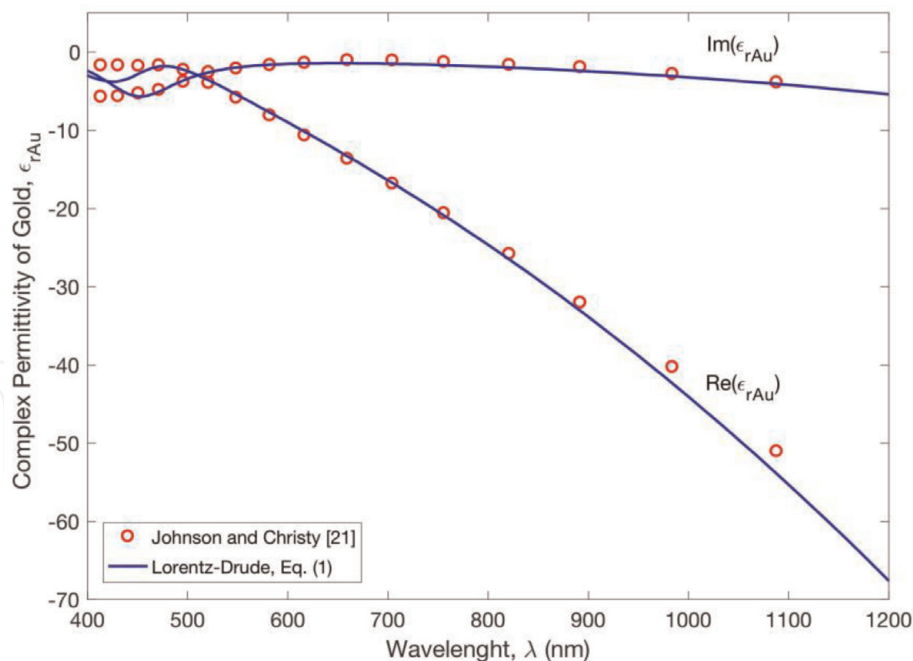


**Figure 4.** Complex permittivity of gold obtained by Lorentz-Drude model of (1) and experimental data of Johnson-Christy [21].

$$Z_s = \frac{TJ_0(Ta)}{2\pi a j \omega \epsilon_{Au} J_1(Ta)}, \quad (2)$$

being  $T = k_0 \sqrt{\epsilon_{rAu}}$  and  $k_0 = \omega \sqrt{\mu_0 \epsilon_0}$ . The boundary condition for the electric field at the conductor surface is  $(\vec{E}_s + \vec{E}_i) \cdot \vec{a}_l = Z_s I$ , where  $\vec{a}_l$  is a unitary vector tangential to the surface of the metal,  $\vec{E}_s$  is the scattered electric field due to the induced linear current  $I$  on the conductor,  $\vec{E}_i$  the incident electric field from the voltage source (**Figure 3**), and  $I$  is the longitudinal current in a given point of the nanodipole.

The integral equation for the scattered field along the length  $l$  of the nanodipole is given by

$$\vec{E}_s(\vec{r}) = \frac{1}{j\omega\epsilon_0} \left[ k_0^2 \int_l \vec{I} g(R) dl' + \int_l \frac{dI}{dl'} \nabla g(R) dl' \right], \quad (3)$$

where  $g(R) = e^{-jk_0 R} / 4\pi R$  is the free space Green's function, and  $R = |\vec{r} - \vec{r}'|$  is the distance between source and observation points. The numerical solution of the problem formulated by (1)–(3) is performed by linear MoM as follows. Firstly, we divide the total length  $L_t = 2L + d$  in  $N = 2N_a + 2$  straight segments, where  $N_a$  is the number of segments in  $L - 0.5d$  with the size  $\Delta L = (L - 0.5d) / N_a$  (white segments in **Figure 3**), and two segments in the middle with the size  $\Delta L = d$  (gray segments in **Figure 3**). Later, the current in each segment is approximated by sinusoidal basis functions. The expansion constants  $I_n$  are shown in **Figure 3** where each constant defines one triangular sinusoidal current. To calculate these constants, we use  $N - 1$  rectangular pulse test functions with unitary amplitude and perform the conventional testing procedure. As a result, the following linear system of equations is obtained:

$$V_m = Z_s I_m \Delta_m - \sum_{n=1}^{N-1} Z_{mn} I_n, \quad m = 1, 2, 3, \dots, N-1, \quad (4)$$

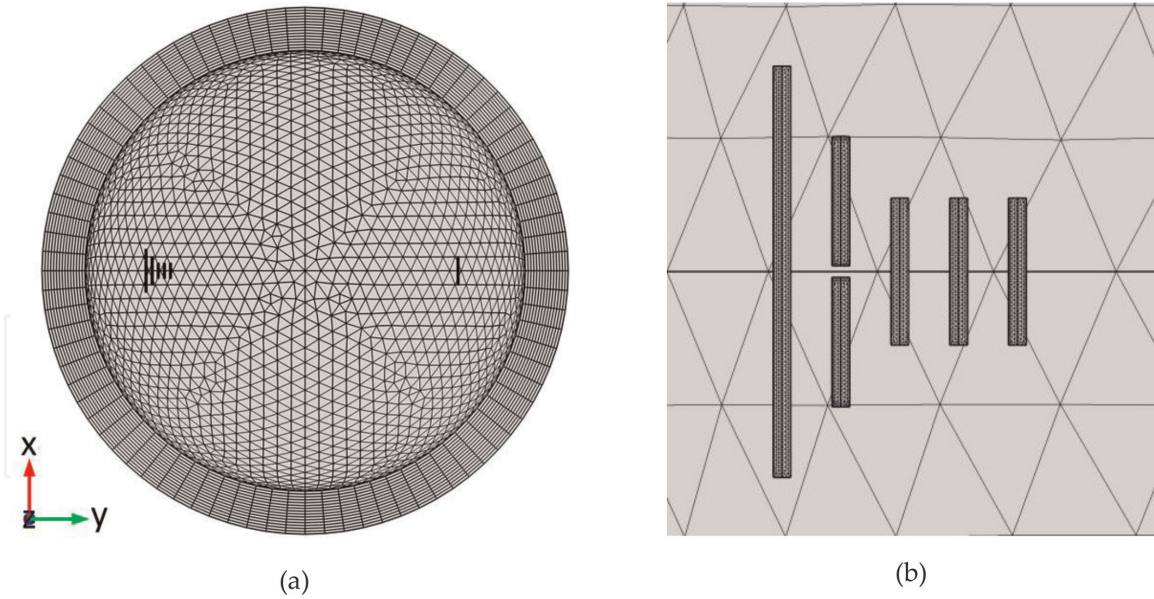


**Figure 5.** Mesh of the problem of **Figure 2** generated in COMSOL. (a) Nanolink mesh and its surroundings. (b) Enlarged Yagi-Uda antenna mesh.

where  $Z_{mn}$  is the mutual impedance between sinusoidal current elements  $m$  and  $n$ ,  $\Delta_m = 1/2[\Delta L_m + \Delta L_{m+1}]$ , and  $V_m$  is non-zero only in the middle of the antenna ( $m = N/2$ ), where  $V_{N/2} = V_s$ . The solution of (4) gives the current along the dipole and the input current  $I_s$ . For  $V_s = 1$  V, the input impedance is  $Z_{in} = 1/I_s = (R_r + R_L) + jX_{in} = R_{in} + jX_{in}$ , where  $R_r$ ,  $R_L$ ,  $R_{in}$ , and  $X_{in}$  are the radiation resistance, loss resistance, input resistance, and input reactance, respectively. The total input power is calculated by  $P_{in} = 0.5\text{Re}(V_s I_s^*) = 0.5(R_L + R_r)|I_s|^2 = 0.5R_{in}|I_s|^2 = P_r + P_L$ ,  $P_r$  is the radiated power, and  $P_L$  the loss power dissipated at the antenna's surface which is calculated by

$$P_L = 0.5\text{Re}(Z_s) \sum_{n=1}^{N-1} |I_n|^2 \Delta_n, \quad (5)$$

The radiated power can be obtained by  $P_r = P_{in} - P_L$ , and the resistances by  $R_r = 2P_r/|I_s|^2$  and  $R_L = 2P_L/|I_s|^2$ . The radiation efficiency is defined by  $e_r = P_r/P_{in} = P_r/(P_r + P_L) = R_r/(R_r + R_L) = R_r/R_{in}$ .

### 3.2 Finite element method

The nanolinks of **Figure 3** were also analyzed numerically by FEM. **Figure 5a** shows the mesh of the nanolink of **Figure 2** modeled in the COMSOL, where the antennas are in a spherical domain of air, with scattering absorbing condition (PLM) applied at their ends. **Figure 5b** shows an enlarged image of the Yagi-Uda nanoantenna mesh and its surroundings.

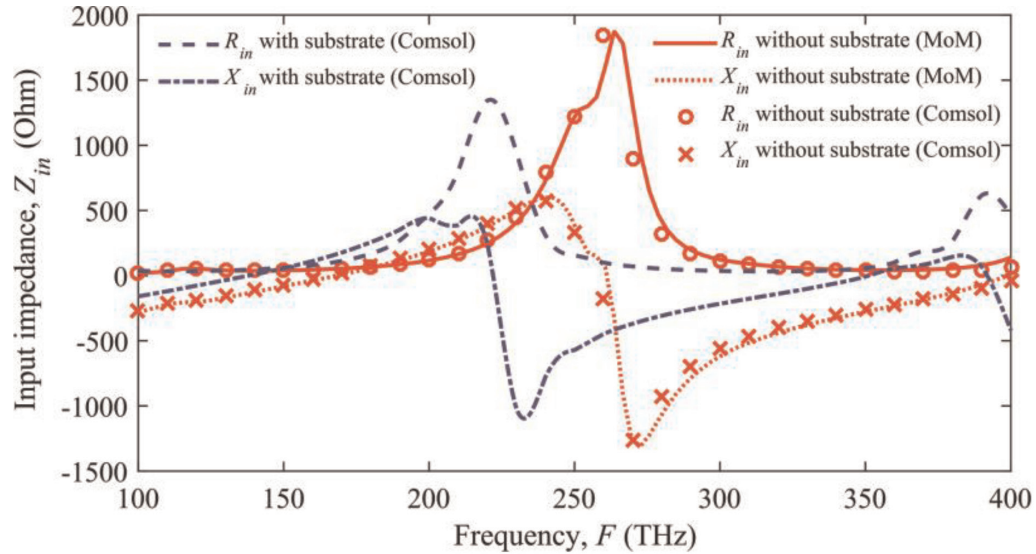
## 4. Numerical results

### 4.1 Isolated antennas in transmitting mode

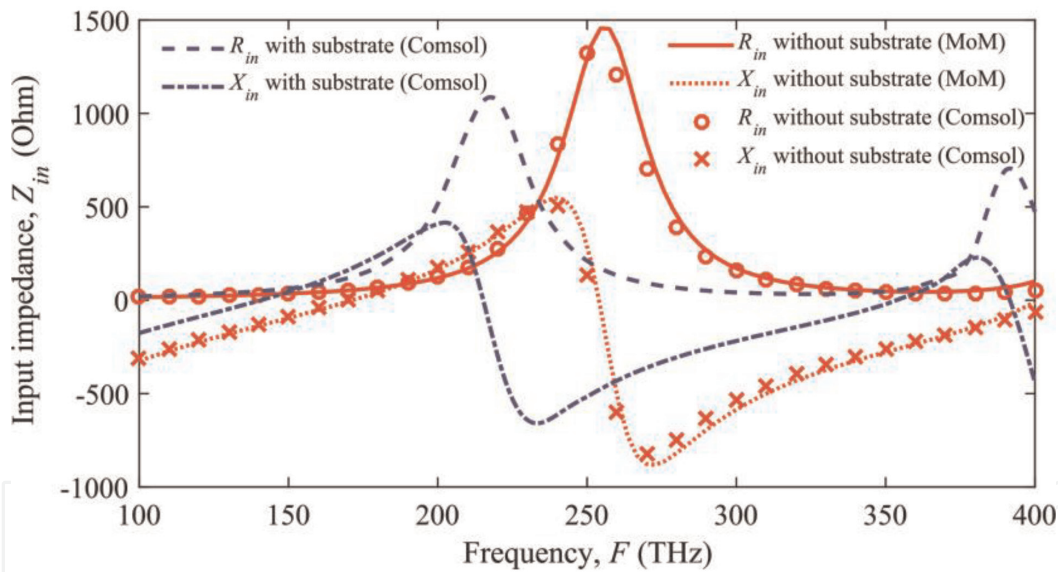
In this section, the transmitting antennas Yagi-Uda and dipole (**Figure 2** without reflector and directors) are analyzed separately. For this analysis, the values of the antennas parameters are those shown in **Table 1**, where with these values the main

Variable	$h_{dT}$	$d_{dT}$	$a$	$h_r$	$h_d$	$h_{dR}$	$d_{dr}$	$d$	$d_{TR}$
Values	220	20	15	700	250	220	20	100	5000

**Table 1.**  
 Nanolink parameters used in simulations. All parameters are in nanometer (nm).



(a)



(b)

**Figure 6.**  
 Input impedance ( $Z_{in}$ ) of the transmitting antennas Yagi-Uda and dipole. (a) Yagi-Uda without substrate, compared to MoM, and with  $\text{SiO}_2$  substrate. (b) Dipole without substrate, compared to MoM, and with  $\text{SiO}_2$  substrate.

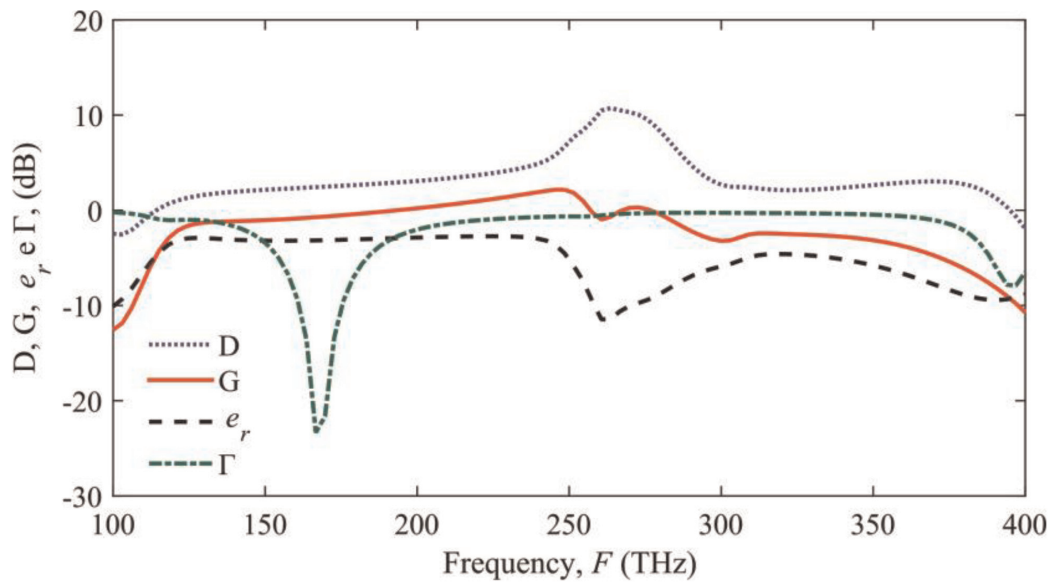
resonances are in the frequency range of 100–400 THz considered. The parameters of the isolated dipole are based on [23] and those of the elements of the Yagi-Uda antenna were chosen so that the reflecting element was larger than the dipole and the smaller dipole directors. In **Table 1**,  $a = a_r = a_{dT} = a_d = a_{dR}$  and  $d = d_{hr} = d_{hd}$ .

**Figure 6** shows the input impedance ( $Z_{in}$ ) for the Yagi-Uda antennas (**Figure 6a**) and dipole (**Figure 6b**). These input impedances were calculated by FEM with the COMSOL software, and by a linear MoM applied to cylindrical plasmonic nanoantennas [18], by coding the mathematical model in Matlab software [24]. We observe a good agreement between these two methods.

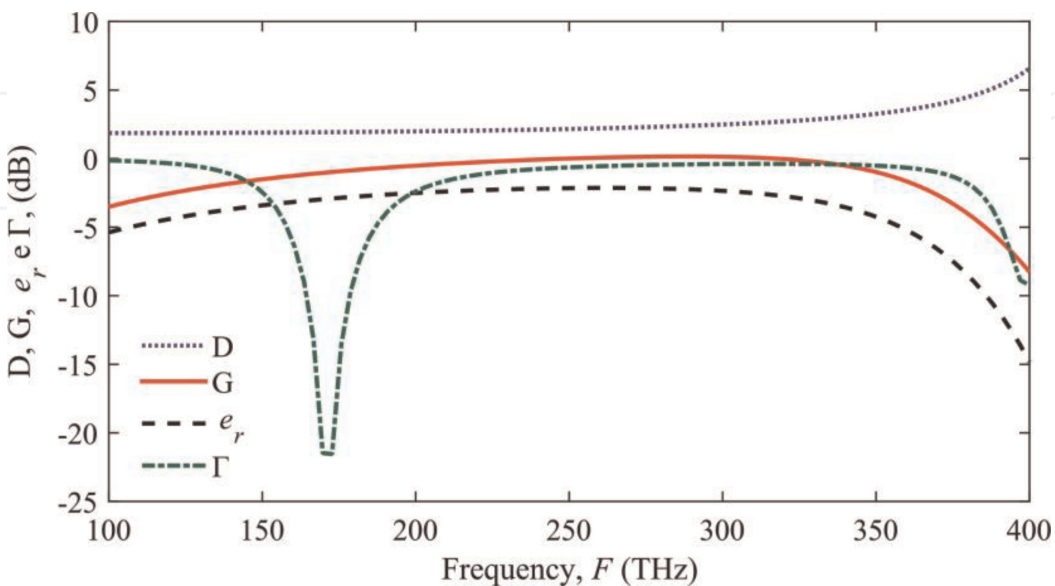
Also, the input impedances of the antennas are calculated for two situations, the first with the antennas in the free space (without substrate) and the second on a  $\text{SiO}_2$  substrate with a permittivity of 2.15.

Comparing the input impedance result between the Yagi-Uda and free-space dipole antennas, it is noted that the first two resonant frequencies are close, which shows that the directors and reflectors do not significantly affect the original resonant frequencies of the isolated dipole. The main differences between these two transmitting antennas are observed near the frequencies of 175 and 260 THz, which correspond physically to the dipole resonances of the reflector and directors, respectively. These resonances can be observed in the distributions of currents in these frequencies, which are not shown here.

**Figure 6** also shows the effect of the substrate in the input impedance and resonant properties of the antennas. It is observed that by placing the antennas on the substrate, their resonances are shifted to smaller frequencies in relation to the



(a)



(b)

**Figure 7.** Directivity ( $D$ ), gain ( $G$ ), radiation efficiency ( $e_r$ ) and reflection coefficient ( $\Gamma$ ) of antennas (a) Yagi-Uda and (b) dipole.

antennas in the free space. This effect of the substrate is similar to that observed in antennas in the microwave regime [25].

**Figure 7** shows the results of directivity ( $D$ ) and gain ( $G$ ), radiation efficiency ( $e_r$ ) and reflection coefficient ( $\Gamma$ ), all in dB, versus frequency for the Yagi-Uda antennas (**Figure 7a**) and dipole (**Figure 7b**). The directivity and gain are calculated in the  $+y$  direction (**Figure 2**). In **Figure 7b** it is observed the conventional characteristic of the isolated dipole, where in a wide range of 150–300 THz one has approximately  $D \approx 1.6$ ,  $e_r \approx 0.6$  e  $G \approx 1$  ( $G = e_r D$ ). In the case of Yagi-Uda (**Figure 7a**), there is a peak of  $D = 12$ , near  $F = 264$  THz, but at this frequency the radiation efficiency is minimal  $e_r \approx 0.1$ , and the gain is ( $G = 0.86$ ). However, if greater gain and efficiency are desired rather than high directivity, the frequency near  $F \approx 240$  THz is more adequate, where the maximum gain is approximately  $G_{max} \approx 1.6$ . The reflection coefficient of both antennas was calculated considering a transmission line with characteristic impedance of  $50 \Omega$  connected to antennas. With this result, it is observed that the best impedance matching for both antennas occurs around the first resonant frequency, however the maximum radiation efficiency occurs at higher frequencies.

**Figure 8** shows the 3D far field gain radiation diagrams of the Yagi-Uda and dipole antennas, calculated at the frequency of 240 THz. It is observed that the maximum gain of the Yagi-Uda ( $G_{max} \approx 1.6$ ) is approximately 60% greater than the maximum gain ( $G_{max} \approx 1$ ) of the dipole. For the case of the Yagi-Uda antenna, the maximum gain occurs in the  $+y$  direction with a small lobe in the  $-y$  direction.

## 4.2 Nanolinks analysis

In this section, we present the results obtained in the analysis of the dipole/dipole nanolinks (**Figure 2**, without reflector and transmitter directors), Yagi-Uda/dipole (**Figure 2**) and Yagi-Uda/Yagi-Uda (**Figure 2**, with the receiving antenna equal to the transmitting antenna) for the frequency range of 100–400 THz. The parameters used for the receiving antennas are same as those of the transmitting antennas, with  $Z_C = 50$  and  $1250 \Omega$  for each nanolink model.

**Figure 9** shows the power transmission in dB (or power transfer function) for the three nanolinks, calculated by the ratio between the power delivered to the  $Z_C$  load and the power delivered by the source  $V_s$  at the transmitting antenna terminals. The results show that the Yagi-Uda/Yagi-Uda nanolink presents a small

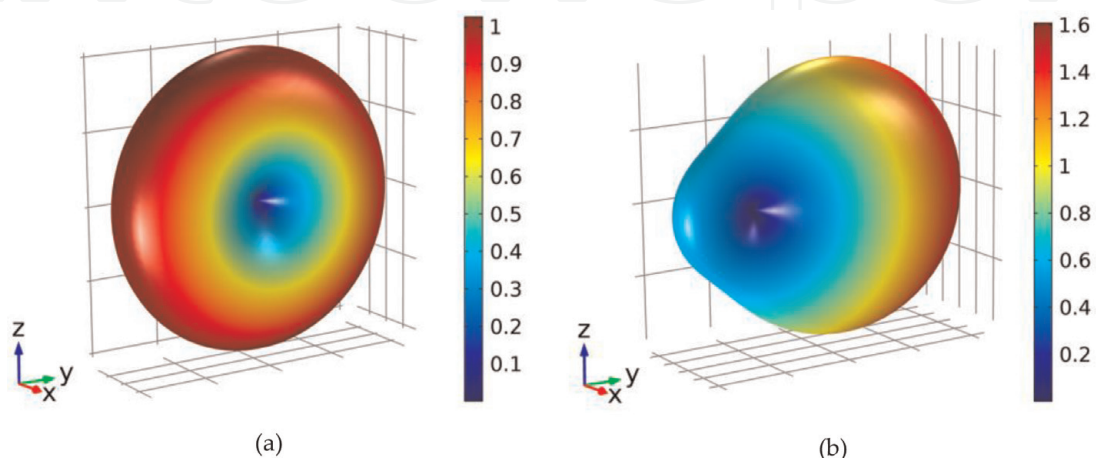


**Figure 8.** 3D far-field gain radiation diagram of (a) dipole antenna, and (b) Yagi-Uda (b), both in  $F = 240$  THz.

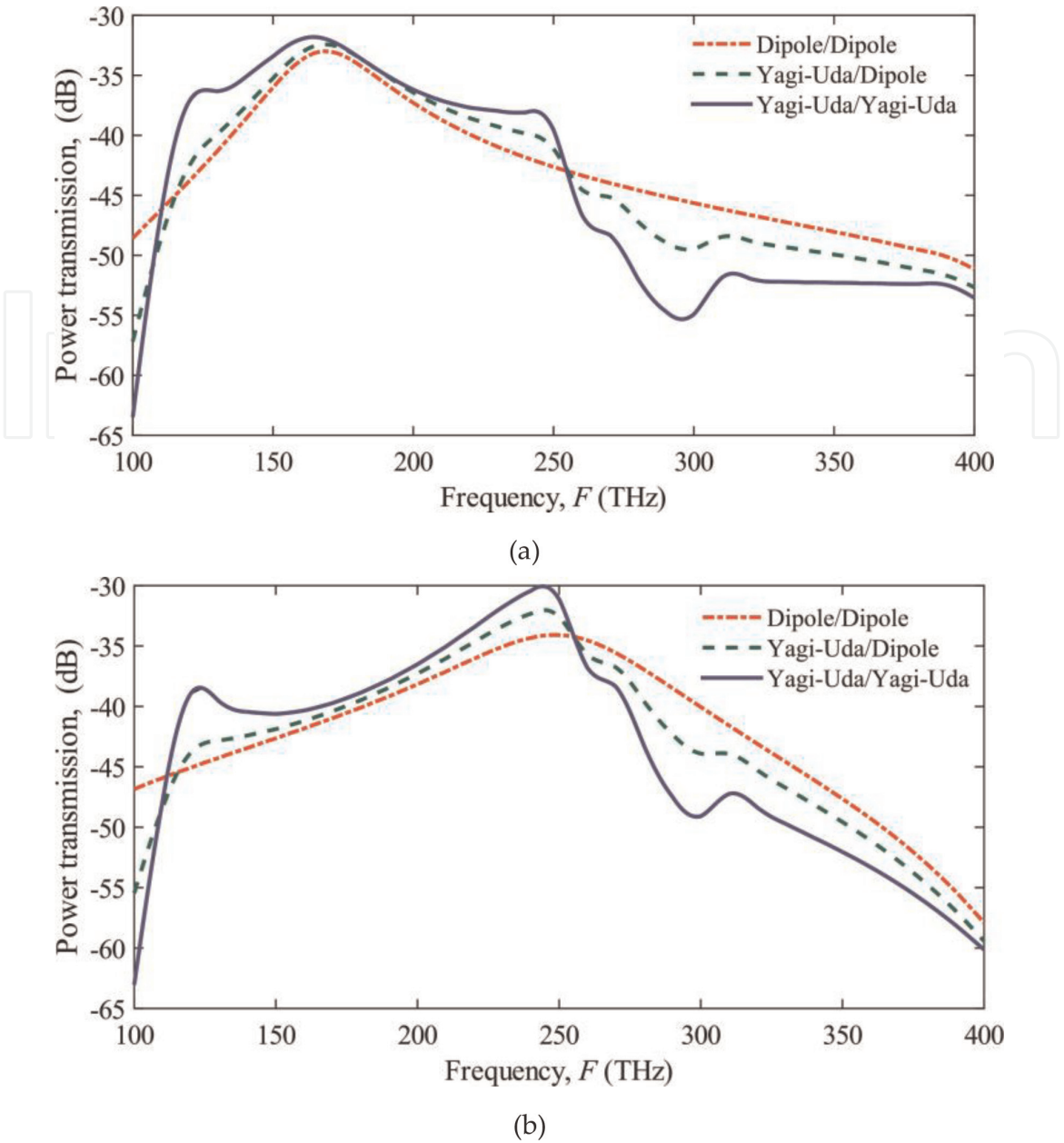


**Figure 9.** Power transmission versus frequency for the dipole/dipole nanolinks, Yagi-Uda/dipole and Yagi-Uda/Yagi-Uda, for  $Z_C = 50$  (a),  $e 1250 \Omega$  (b).

improvement in power transmission, at some frequency points, in relation to the dipole/dipole and Yagi-Uda/dipole nanolinks. In addition, it can be observed that the links can operate with good transmission power at the frequency points 170 and 240 THz, for  $Z_C$  equal to 50 and 1250  $\Omega$ , respectively, where the power transmission are maximum.

**Figure 10** shows the magnitude and phase of the electric near field, which is defined by  $E = 20 \log_{10}(|\text{Re}(E_x)|)$ , in the plane  $z = 25$  nm, of the dipole/dipole nanolinks (a, b), Yagi-Uda/dipole (c, d) and Yagi-Uda/Yagi-Uda (e, f). The receiver antennas are positioned at a distance  $d_{TR} = 5 \mu\text{m}$  from the transmitting antennas, with  $F = 170$  THz and  $Z_C = 50 \Omega$  for the fields of figures (a), (c) and (e), and with  $F = 240$  THz and  $Z_C = 1250 \Omega$  for the cases of figures (b), (d) and (f). In all types of nanolinks shown in this figure, the radiated wave can be visualized by propagating from the transmitting antennas to the receiving antennas, with the appropriated wavelength. It is observed the amplitude decay of the electric field with the distance and the decrease of the wavelength with the increase of the frequency.

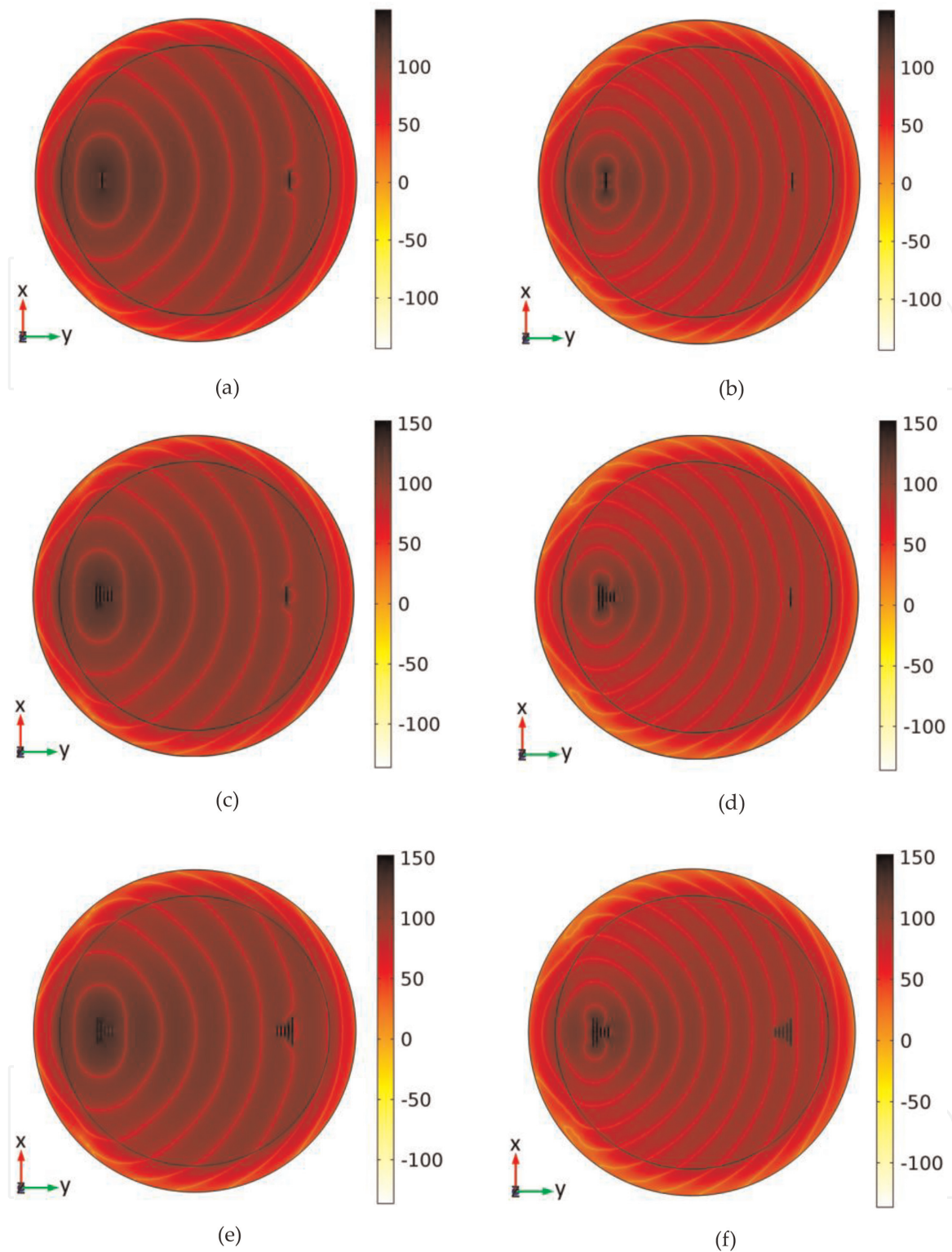


**Figure 10.** Electric near field distribution of the magnitude and phase ( $E = 20 \log_{10}(|\text{Re}(E_x)|)$ ), in the plane  $z = 25$  nm, of the dipole/dipole nanolinks (a, b), Yagi-Uda/dipole (c, d) and Yagi-Uda/Yagi-Uda (e, f). The receiver antennas are positioned at  $5 \mu\text{m}$  from the transmitting antennas, with  $F = 170$  THz and  $Z_C = 50 \Omega$  for figures (a), (c) and (e), and with  $F = 240$  THz and  $Z_C = 1250 \Omega$  for figures (b), (d) and (f).

## 5. Conclusions

It was presented in this work, a comparative analysis of nanolinks formed by Yagi-Uda and dipole plasmonic nanoantennas, where was investigated the power transmission for Yagi-Uda/Yagi-Uda, Yagi-Uda/dipole and dipole/dipole nanolinks

types. These nanolinks were numerically analyzed by method of moments and finite element method. The results show that the Yagi-Uda/Yagi-Uda nanolink presents a small improvement in power transmission, at some frequency points, in relation to the other cases. In addition, the three links can operate with good power transmit at different frequency points, varying the load impedance of the receiving antenna, which is of great importance for future applications in nanoscale wireless communication. In future work, we intend to feed these nanolinks by more realistic sources, such as gaussian beams, to verify their influence on power transmission results.

## Acknowledgements

The authors would like to thank the Mr. Mauro Roberto Collato Junior Chief Executive Officer of the Junto Telecom Company for the financial and emotional support to this project.

## Conflict of interest

The authors declare that there is no conflict of interests regarding the publication of this work.

## Author details

Karlo Queiroz da Costa<sup>1\*</sup>, Gleida Tayanna Conde de Sousa<sup>1</sup>, Paulo Rodrigues Amaral<sup>1</sup>, Janilson Leão Souza<sup>2</sup>, Tiago Dos Santos Garcia<sup>1</sup> and Pitther Negrão dos Santos<sup>1</sup>

<sup>1</sup> Department of Electrical Engineering, Federal University of Para, Belém-PA, Brazil

<sup>2</sup> Federal Institute of Education, Science and Technology of Para, Tucuruí-PA, Brazil

\*Address all correspondence to: karlo@ufpa.br

## IntechOpen

© 2019 The Author(s). Licensee IntechOpen. This chapter is distributed under the terms of the Creative Commons Attribution License (<http://creativecommons.org/licenses/by/3.0>), which permits unrestricted use, distribution, and reproduction in any medium, provided the original work is properly cited. 

## References

- [1] Novotny L, Hecht B. Principles of Nano-Optics. New York: Cambridge; 2006
- [2] Maier SA. Plasmonics: Fundamentals and Applications. New York: Springer; 2007
- [3] Grober RD, Schoelkopf RJ, Prober DE. Optical antenna: Towards a unity efficiency near-field optical probe. *Applied Physics Letters*. 1997;**70**: 1354-1356
- [4] Pohl DW. Near field optics as an antenna problem. Second Asia-Pacific Workshop on Near Field Optics. Beijing, China; 1999. pp. 9-21
- [5] Novotny L. From near-field optics to optical antennas. *Physics Today*. 2011; **64**(N7):47-52
- [6] Bharadwaj P, Deutsch B, Novotny L. Optical antennas. *Advances in Optics and Photonics*. 2009;**1**:438-483
- [7] Novotny L, Hulst NV. Antennas for light. *Nature Photonics*. 2011;**5**:83-90
- [8] Alù A, Engheta N. Theory, modeling and features of optical nanoantennas. *IEEE Transactions on Antennas and Propagation*. 2013;**61**(N4):1508-1517
- [9] Giannini V, Dominguez AIF, Heck SC, Maier SA. Plasmonic nanoantennas: Fundamentals and their use in controlling the radiative properties of nanoemitters. *Chemical Reviews*. 2011;**111**:3888-3912
- [10] Krasnok AE. Optical nanoantennas. *Physics-Uspekhi*. 2013;**56**(N6):539-564
- [11] Berkovitch N, Ginzburg P, Orenstein M. Nano-plasmonic antennas in the near infrared regime. *Journal of Physics: Condensed Matter*. 2012;**24**: 073202
- [12] Atwater HA, Polman A. Plasmonics for improved photovoltaic devices. *Nature Materials*. 2010;**9**:205-213
- [13] de Souza JL, da Costa KQ. Broadband wireless optical nanolink composed by dipole-loop nanoantennas. *IEEE Photonics Journal*. 2018;**10**:1-8
- [14] Alù A, Engheta N. Wireless at the nanoscale: Optical interconnects using matched nanoantennas. *Physical Review Letters*. 2010;**104**:213902
- [15] Solís D, Taboada J, Obelleiro F, Landesa L. Optimization of an optical wireless nanolink using directive nanoantennas. *Optics Express*. 2013;**21**: 2369-2377
- [16] Bellanca G, Calò G, Kaplan A, Bassi P, Petruzzelli V. Integrated Vivaldi plasmonic antenna for wireless on-chip optical communications. *Optics Express*. 2017;**25**:16214-16227
- [17] Yang Y, Li Q, Qiu M. Broadband nanophotonic wireless links and networks using on-chip integrated plasmonic antennas. *Scientific Reports*. 2016;**6**:19490
- [18] da Costa KQ, Dmitriev V. Simple and efficient computational method to analyze cylindrical plasmonic nanoantennas. *International Journal of Antennas and Propagation*. 2014;**2014**. 8 pages
- [19] COMSOL Multiphysic 4.4. COMSOL Inc. Available from: <http://www.comsol.com>
- [20] Sabaawi AMA, Tsimenidis CC, Sharif BS. Analysis and modeling of infrared solar rectennas. *IEEE Journal of Selected Topics in Quantum Electronics*. 2013;**19**(N3): 9000208

[21] Johnson PB, Christy RW. Optical constants of the noble metals. *Physical Review B*. 1972;6:4370-4379

[22] Hanson GW. On the applicability of the surface impedance integral equation for optical and near infrared copper dipole antennas. *IEEE Transactions on Antennas and Propagation*. 2006;54(N12):3677-3685

[23] Da Costa KQ, Dmitriev V. Radiation and absorption properties of gold nanodipoles in transmitting mode. *Microwave and Optical Technology Letters*. 2015;57:1-6

[24] Matlab Software. Available from: <https://www.mathworks.com/products/matlab.html>

[25] Balanis CA. *Antenna Theory- Analysis and Design*. 3rd ed. New Jersey: John Wiley & Sons; 2005